Mechanical stability for nanostructured Sn- and Si-based anodes

K.E. Aifantis [a,b,*], S.A. Hackney [a,c]

[a] Lab of Mechanics and Materials, Aristotle University of Thessaloniki, Thessaloniki, Greece
[b] Physics Department, Michigan Technological University, Houghton, MI, USA
[c] Materials Science and Engineering, Michigan Technological University, Houghton, MI, USA

ABSTRACT

The most promising materials that can be used as anodes in next generation rechargeable Li batteries are Sn and Si. Upon lithiation, however, both Sn and Si experience a 300% volume expansion, which results in significant fracture, and therefore their commercial use is inhibited. Extensive experimental research has yielded that embedding or attaching Si or Sn nanoparticles in a carbon/graphite matrix diminishes their mechanical damage and allows for electrochemical stability. The present study will show that linear elasticity can predict the capacity retention of such nanocomposites by predicting their mechanical stability upon Li-insertion. In particular (i) a previously developed theoretical model will be related to experimental observations on Si/sol–gel-graphite nanocomposite anodes, (ii) electron microscopy images will be presented on the fracture of cycled SnO_2/C nanopowders, and a theoretical model will be applied to predict the SnO_2 particle dimensions that will limit such fracture.

© 2010 Elsevier B.V. All rights reserved.

1. Introduction

Secondary Li batteries are the most rapidly growing high energy density power sources; their applications ranging from hybrid and electric vehicles, to biomedical implantable devices [1]. Commercial anodes for Li batteries comprise of graphite since it offers both electrochemical and mechanical stability. One of the drawbacks, however, is that graphite has a low Li intercalation (Li_xC_6, where $0 < x < 1$), and therefore provides a capacity of 372 mAh g^{-1} [2] upon lithiation.

About the same time that graphite was proposed as a stable anode, experimental research [3] yielded that the most promising anodic materials are Si and Sn, which allow for capacities of 4200 mAh g^{-1} and 990 mAh g^{-1}, respectively, upon the formation of Li intermetallics [4]. These high capacities are partly attributed to the higher Li-intercalation in these materials, namely Li_xSn and Li_xSi, where $0 < x \leq 4.4$. Despite their unique electrochemical properties, however, Sn and Si cannot be used commercially, as their mechanical behaviour pays the penalty of their high reactivity with Li. In particular, during maximum Li insertion, Si and Sn experience volume expansions of 300% [4]. As a result during electrochemical cycling (continuous insertion and de-insertion of Li) the anodes expand (lithiation) and contract (de-lithiation) leading to fracture. This fracture produces active material that is no longer in electri-

cal contact with the remainder of the electrode, which therefore becomes unable to respond to the applied voltages necessary to recharge or control the discharge of the battery.

The capacity of bulk Sn and Si, therefore, becomes negligible after the first few cycles. At the nanoscale, however, deformation mechanisms are less severe, and better capacity retentions have been achieved. In [5] it was illustrated that during the first Li-insertion the capacity of Sn nanoparticles (50–200 nm in diameter) was 990 Ah g^{-1}, but it dropped to 210 mAh g^{-1} after 20 cycles. Similar trends were shown for Si nanoclusters that gave a starting capacity of 2400 mAh g^{-1}, which reduced to 525 mAh g^{-1} after fifty cycles [6]. Post mortem transmission electron microscopy images document that this large capacity reduction during cycling is attributed to the severe fracture that results from the volume expansion of the Sn and Si nanopaticles.

The most effective way to constrain/accommodate these expansions is to embed/attach the active materials with respect to Li, in a less active matrix.[1] The matrix constrains/buffers the volume expansions, and also protects the active site surface from electrochemical damage. One of the most effective such matrices is carbon/graphite, since once maximum Li-insertion takes place in the active site, additional Li can be intercalated by the carbon.

Niu and Lee [7] were able to achieve capacities greater than 2400 mAh g^{-1} for 20 cycles by embedding Si nanoparticles in a

---

* Corresponding author at: Lab of Mechanics and Materials, Aristotle University of Thessaloniki, Thessaloniki, Greece. Tel.: +30 2310 995921; fax: +30 2310 995921.
E-mail address: k.aifantis@mom.gen.auth.gr (K.E. Aifantis).

[1] By embedding the active material is fully surrounded by the matrix, whereas by attaching the active material is attached on the surface by the matrix forming an island structure.

sol–gel-graphite matrix, while Derrien et al. [8] were able to attain a capacity of 500 mAh g^{-1} for 100 cycles by embedding Sn nanoparticles in graphite. In addition, to embedding the nanoparticles, it was shown that attaching Sn particles on an amorphous carbon surface, increased the carbon capacity by 85% [9]. Instead of using carbon or graphite as the matrix, cellulose fibers have also been successfully employed; Si nanoparticles attached on cellulose gave capacities of 1300 mAh g^{-1} for 30 cycles [10], and Sn attached on cellulose gave a capacity of 500 mAh g^{-1} for 40 cycles [11]. Such Sn and Si based anode materials are usually referred to as active/inactive composites, since the Sn and Si are significantly more active with respect to Li as compared to the matrix. It is clearly seen that using such nanocomposite systems as anodes results in a much better capacity retention than using Sn or Si in their pure form [5,6]. A more detailed overview on various configurations and materials chemistries that are being considered as next generation anodes in Li batteries can be found in [1].

It should be noted, however, that not only materials chemistry, but also the particle size and the volume fraction of the active sites affect the capacity. In [7] for example, three different Si/sol–gel-graphite anodes were tested, with a different Si content. The capacity retention was the best for the anode with the lowest Si content. Furthermore, the promising Sn/graphite anode presented in [8] had a mean Sn particle diameter of 35 nm, whereas, earlier studies, that used similar Sn/graphite nanocomposites, but with a Sn average diameter greater than 100 nm gave very poor capacity retentions [12].

Although the existing experimental evidence can provide some insight towards selecting appropriate particles size and volume fractions, design criteria can be obtained only through the development of theoretical models that can predict electrochemical and/or mechanical stability. In the present study, therefore, the high capacity retention that can be obtained for active/inactive anodes will be related to their enhanced mechanical stability. The theoretical predictions that will be deduced through linear elasticity and energy considerations will be directly used to interpret existing and new experimental data.

2. Mechanical models developed for Li anode fracture

Although there exist myriad studies on the experimental aspects of Li-electrodes, there is limited work that focuses on the mechanical issues of such systems, despite the experimental indications that these systems fail due to severe damage and fracture [4,13]. Before, therefore, Sn and Si based anodes can be used commercially their fracture mechanisms must be understood.

Wolfenstine [14] employed linear elasticity to predict that the particle size of Sn that will result in no fracture, during lithiation, is below its unit cell size. Huggins and Nix [15], however, predicted that the particle size that will inhibit fracture is below 0.35 μm for brittle materials and 8 μm for ductile materials, which however, is not consistent with experimental evidence. This discrepancy from experiments is most likely due to the fact that the work in [15] was based on the fracture analysis model of a thin film configuration and, hence, the internal stress development and fracture of an epitaxial thin film on a compliant substrate [16] was analyzed, instead of the actual radial symmetry that is present in active/inactive nanocomposites.

The mechanics challenges that arise for electrodes comprised of active nanoparticles embedded in a matrix were initially undertaken in [17–19], through the development of simple physically based linear elasticity and fracture mechanics models. The goal was to establish preliminary easy-to-use material/component design criteria for nanostructured anodes [20] with optimum capacity, strength, and electrochemical stability. In particular, under con-
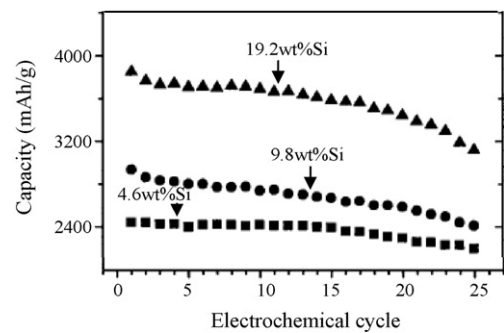

Fig. 1. Experimental data exhibiting the capacity fade of nano-Si embedded in a sol–gel graphite matrix (taken from [7]); lower Si content has a lower capacity fade.

tinuous electrochemical cycling (nano) cracking takes place at the particle–matrix interface and a (nano) damage zone is developed as documented by transmission electron microscopy observations [17,21]. On assuming that this damage zone is comprised by a number of radial cracks, Aifantis et al. [20] were able to derive stability criteria for the crack growth depending on the geometry assumed for the active nanoparticles (spheres, cylinders or disks), and the associated boundary conditions.

Strain considerations for radial geometries for the active sites have also been recently examined in [22], which looked at moderately expanding cathodes, with geometries similar to those advanced previously in [17–20], but also accounted for stress-assisted diffusion similarly as in [23]. A more recent study [24] highlights how stresses are built up in porous electrodes which are an agglomerate of active particles, the electrolyte, and the inactive material.

3. Volume fraction considerations in Si-sol–gel-graphite (Si-SGG) anodes

In order to understand the effect that the Si volume fraction has in the overall capacity retention, Niu and Lee [7] considered three different anodes: 19.2 wt%Si-SGG, 9.8 wt%Si-SGG and 4.8 wt%Si-SGG. As seen in Fig. 1 the nanocomposite with the highest Si content (19.2 wt%Si) gave a higher initial capacity, since it contained more active material, but after 25 cycles the capacity decreased by 18%. The lowest Si content (4.8 wt%Si) anode gave a lower initial capacity which, however, remained stable for 25 cycles. In this section it will be shown that this correlation between Si content and capacity retention is attributed to the underlying mechanical stability.

In [18] linear elasticity and axial symmetry was employed to study the fracture of nanocomposite anodes in which spherical active sites were embedded in a matrix; a unit cell is shown in Fig. 2. The fracture that occurs during electrochemical cycling was accounted for by considering a damage zone at the active site/matrix interface. This zone was characterized by multiple radial cracks of length ρ-a, whose opening tensile stress was $\sigma_{\theta\theta}$. Earlier work by Dempsey and co-workers [25,26] concluded that the energy release rate (G) during cracking in such geometries is given by

$$G = \frac{(1 - v_m)a^4 p^2}{2nE_m\rho^3}\left[\frac{(b+2\rho)(b-\rho)}{b^2 + b\rho + \rho^2}\right]^2,$$

(1)

where a and b are the radii of the active site and matrix, ρ is the crack radius, v_m and E_m are the Poisson's ratio and elastic modulus of the matrix, and n is the number of radial cracks. p is the internal pressure that the active site exerts onto the matrix upon its 300% volume expansion during maximum Li-insertion and was
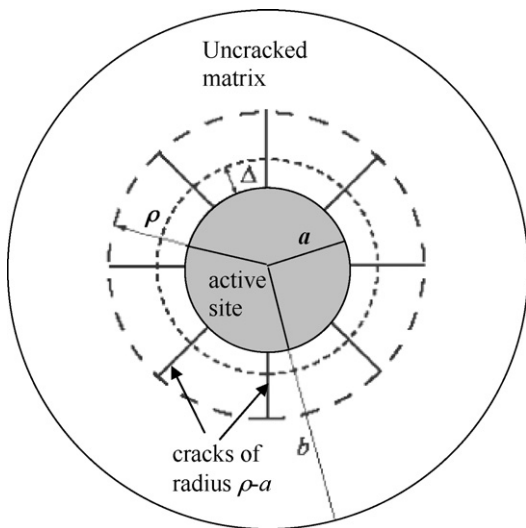
Fig. 2. Configuration of unit cell used in analysis; *a* and *b* are the radii of the active site and matrix, Δ is the free expansion of the active site if it were not constrained (by the matrix), and ρ is the crack radius.
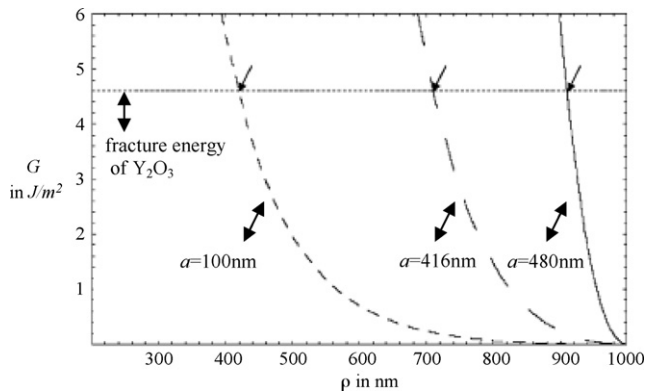

Fig. 3. Griffith's criterion for various volume fractions (*b* is kept 1000 μm), of Si nanospheres (with radius *a*) embedded in a Y_2O_3 matrix. Arrows indicate the crack radius at which fracture will stop.

computed as [19]

$$p = \Delta \left\{ \frac{a^2}{\rho E_m} \left[\frac{\rho}{a} - \frac{(1 - \nu_m)}{2} - \frac{3(1 - \nu_m)\rho^2}{2(b^2 + b\rho + \rho^2)} \right] + \frac{(a + \Delta)E_s}{1 - 2\nu_s} \right\}^{-1},$$

(2)

where ν_s and E_s are the Poisson's ratio and elastic modulus of the active site and Δ corresponds to the distance the active site would expand to if it was not constrained by the matrix. By inserting, therefore, the material parameters for Si and C in Eqs. (1) and (2) the energy released during fracture in Si–C nanocomposites can be predicted. In order to capture the effects of the volume fractions of the Si active sites, *b* was kept constant at 1000 μm, while *a* was allowed to attain values of 100 nm, 216 nm and 480 nm so as to vary the volume fraction. In Fig. 3, in addition to the energy release rates for various volume fractions, the fracture energy of the matrix is also plotted. Therefore, based on Griffith's criterion, the crack radius at which fracture will stop is the point at which the energy release rate, *G*, during crack growth, exceeds the fracture energy of the matrix. Based on Fig. 3 it can be seen that as the volume fraction of the active site decreases, cracking will stop at shorter distances.[2]

This implies that anodes containing low active site volume fractions experience less cracking and therefore the anode connectivity is not significantly disrupted during cycling, allowing hence for the material to respond to the applied voltages during cycling and, hence, providing, therefore, a stable capacity retention.

Despite the purely mechanical framework employed, the aforementioned predictions by Aifantis et al. [20] are qualitatively in agreement with the experimental evidence shown in Fig. 1, in which it is clearly seen that the lowest Si content anode allowed for a more stable capacity retention than the higher Si content anodes. More mathematical details of the model presented above can be found in [18,20].

4. Aspect ratio of SnO₂ particles SnO₂–C nanocomposites anodes

In this section new experimental evidence will be presented, that documents the Sn aspect ratio effect in capacity retention. This will be done by examining the microstructure of Sn/C nanopowders that can be used as anodes.[3]

Fig. 4a and b depicts Sn particles attached on multiwalled carbon nanotubes [27]. It can be seen that the large Sn particles covered the whole nanotube surface, forming a type of thin film layer. Upon the first Li-insertion the capacity was above 500 mAh g^{-1}, however, during the second charge the capacity was negligible. It was anticipated that this significant capacity drop was due to fracture and, therefore, scanning (SEM) and transmission (TEM) electron microscopy was performed after the first cycle. It was indeed seen that significant cracks formed on the Sn layer (Fig. 4c), while further TEM indicated that the large Sn particles had fractured into multiple nanoparticles (Fig. 4d).

In addition to depositing Sn in the form of a thin layer on carbon, it is also possible to attach Sn islands on amorphous carbon obtaining a microstructure of fine active particles dispersed on the carbon surface. For this case, the Sn attaches in the form of SnO₂ [27], and thus far a fabrication method that allows the attachment of pure Sn on amorphous carbon does not exist. Aifantis et al. [9] cycled the material of Fig. 5 and observed a stable capacity of 385 mAh g^{-1} for 500 cycles. It should be noted that the capacity of the Vulcan-X72 that was used as the matrix was 180 mAh g^{-1}, prior to the attachment of the SnO₂. A 85% capacity increase, hence, resulted by the addition of 8 wt%Sn. Such an increase in capacity through the addition of such a low wt%Sn has not been observed before; note for example that in [8] 50% Sn metal was added to increase the graphite capacity by 40%. The electrochemical stability observed for the material in Fig. 5 indicates that the Sn nanoparticles did not experience fracture upon continuous Li-insertion and de-insertion, similar to that which occured for the Sn film layer of Fig. 4.

The mechanics based advantage of the island design (Fig. 5) relative to the continuous thin film geometry (Fig. 4) is related to the resistance of the Sn island particles to delamination during volume expansion. This resistance to delamination of islands compared to thin films arises from the stress reduction associated with free boundary conditions and is accentuated at a high aspect ratio (island height)/(island width), or *H/L*. For a given strain due to island volume expansion on an infinitely stiff substrate, it is proposed that the critical delamination compressive stress concept developed in [28,29] may be adapted to the island geometry as

$$\sigma_c = \frac{(15)E}{12(1 - \nu^2)} \left(\frac{2H}{L} \right)^2,$$

(3)

---

[2] The fracture energy of C could not be found in the literature and therefore Y_2O_3 was used as the matrix; the same qualitative results, however, would be true for any matrix material.

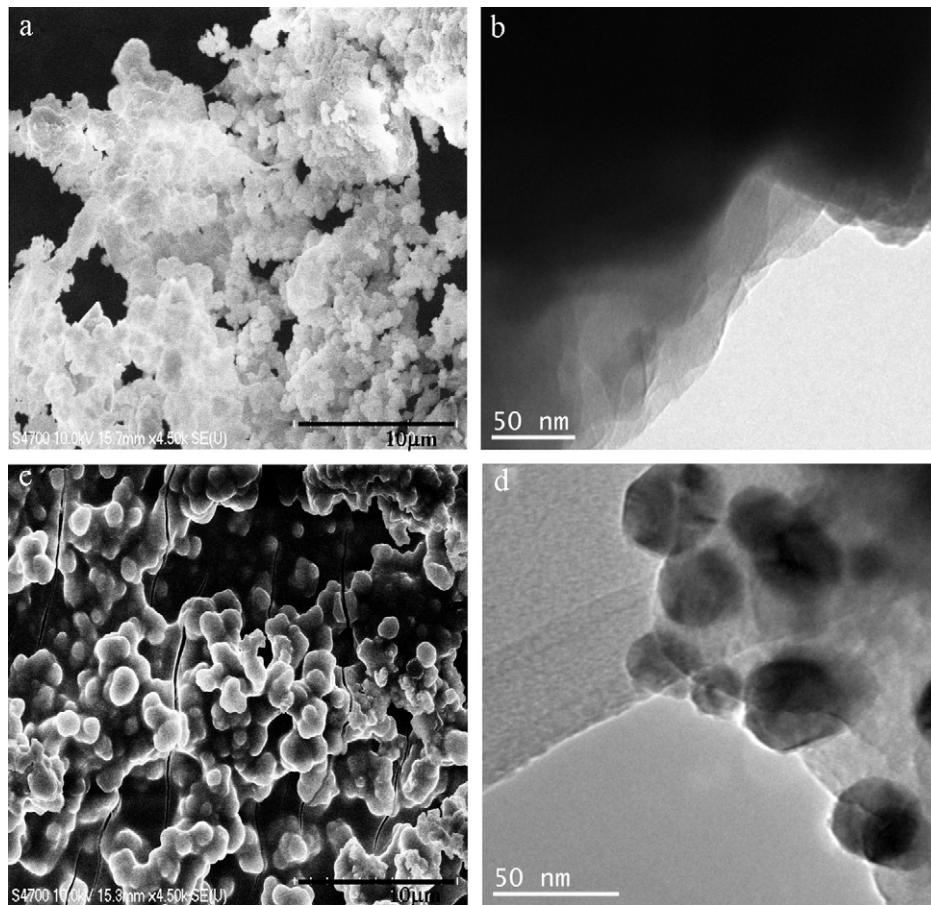[3] These materials were fabricated and presented in [27].

Fig. 4. (a) SEM image of as prepared Sn attached on multi-walled carbon nanotubes; Sn appears as the bright phase, (b) TEM image of as prepared Sn attached on multi-walled carbon nanotubes; Sn appears as black phase, (c) SEM image after first de-lithiation indicating macro-cracks; (d) TEM image after the first de-lithiation, indicating nanoscale fractured particles. SEM scale bars are 10 μm.

where H is the island half thickness and L is the island half length. Therefore, if the compressive stress in the island exceeds the critical delamination stress, then the island will detach and most likely fail to contribute to the electrochemical activity. It can, therefore, be understood that the aspect ratio (H/L) is critical to the mechanical stability of the island geometry. In order to test the idea that the free surface boundary conditions associated with the island geometry will reduce the compressive stress relative to that in a continuous thin film, a two dimensional elasticity solution is pursued for the geometry shown in Fig. 6. The stresses and displacements that the island experiences are taken to be given by the biharmonic Marguerre solutions [30] as

$$\sigma_{xx}(x,y) = \frac{E}{1-\nu^2}\left(-\frac{d^3\Psi}{dx^2 dy} + \nu\frac{d^3\Psi}{dy^3}\right), \quad \sigma_{yy}(x,y) = \frac{E}{1-\nu^2}\left((1+\nu)\frac{d^3\Psi}{dx^2 dy} + \frac{d^3\Psi}{dy^3}\right),$$

$$\sigma_{xy}(x,y) = \frac{E}{1-\nu^2}\left(\frac{d^3\Psi}{dx^3} + \frac{d^3\Psi}{dxdy^2}\right), \quad u_x(x,y) = \frac{1+\nu}{1-\nu}\left(\frac{d^2\Psi}{dxdy}\right)$$

(4)

where the energy functional Ψ is of the form

$$\Psi = \cos(\beta_n x)(A\sin h(\beta_n y) + B\cos h(\beta_n y) + C\beta_n y\sin h(\beta_n y)); \quad (5)$$
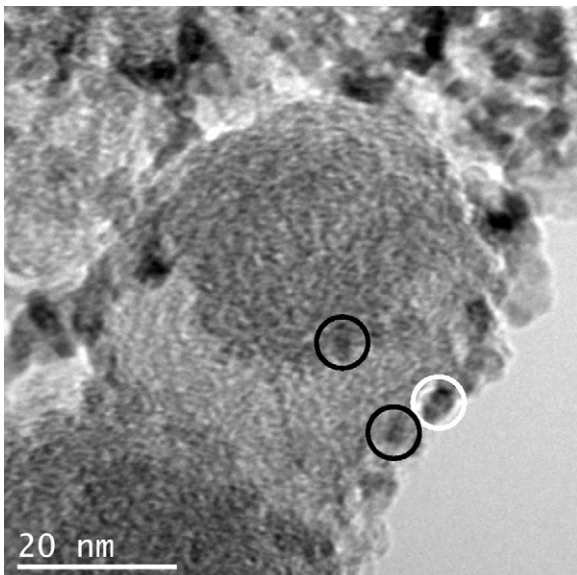

Fig. 5. 8 wt%Sn-Vulcan C nanopowder prior to electrochemical cycling. Dark areas indicate Sn rich areas. Representative Sn islands are contained in circles.
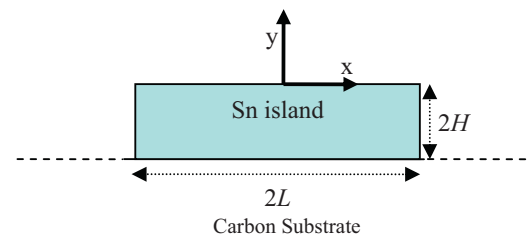

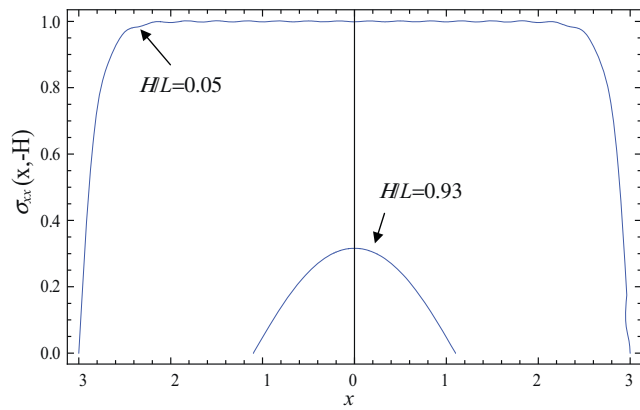**Fig. 6.** Schematical representation of Sn/C island microstructure.

Fig. 7. Comparing the normalized compressive stress for different H/L values.

Fig. 8. In order for the islands to remain attached to the carbon, their height/length ratio (H/L) must be greater than 0.3.

where, $\beta_n = n\pi/2L$ (n = odd), while the constants A, B, are found from the boundary conditions

$$\sigma_{xx}(L, y) = 0, \quad \sigma_{yy}(x, 0) = 0, \quad \sigma_{xy}(x, 0) = 0, \tag{6}$$

as

$$A = 0 \text{ and } B = -\frac{2\nu C}{1 + \nu}$$

C is found from the definition of the displacement at the island:carbon interface as a linear function of x so that $\Delta x/L = u_x(y = -2H)$. Expanding the displacement as a Fourier series in which C becomes a Fourier coefficient (and thus a function of the Fourier index, n, the various values of C_n may be determined from Eq. (7)):

$$\int_{-L}^{L} \left(\frac{\Delta x}{L} \sin(\beta_n x) \right) dx = \int_{-L}^{L} \left[(u_x(x, -2H)) \sin(\beta_n x) \right] dx \tag{7}$$

where Δ, as in the previous sections, denotes the unconstrained expansion of the Sn island.

Hence,

$$C_n = \frac{32L^3(\nu - 1)\Delta \sin(n\pi/2)}{n^3\pi^3(n\pi) \left[n\pi H(1 + \nu)\cos h(n\pi H/L) - L(\nu - 1)\sin h(n\pi H/L) \right]}$$

Insertion of the constants of integration, A, B and C, in Eq. (5) and then in Eq. (4) allows the determination of the compressive stress σ_{xx}; Δ is taken to be a proportional function of the strain associated with the maximum constraint to island expansion, ε, $\Delta = \varepsilon L$. The form of the spatial variation in the normalized compressive stress along x at $y = (-H)$ for two different H/L values at a given island volume is shown in Fig. 7. It may be seen that the average and maximum amplitude of the compressive stress is reduced in value when H/L is large as compared to when it is small.

Application of the criteria for delamination described in Eq. (3) to this elasticity solution is carried out by calculating the average compressive stress in an island and then comparing this average stress to the critical stress for delamination. This procedure is developed in Fig. 8 for an island structure with an individual Sn island volume of 16.75 nm³ is obtained by calculating the average compressive stress in an island. This average compressive stress is substituted into Eq. (3) giving

$$\frac{2L}{8HL^2} \int_{-2H}^{0} \int_{-L}^{L} \sigma_{xx} dx dy = \frac{15E}{12(1 - \nu^2)} \left(\frac{2H}{L} \right)^2 \tag{8}$$
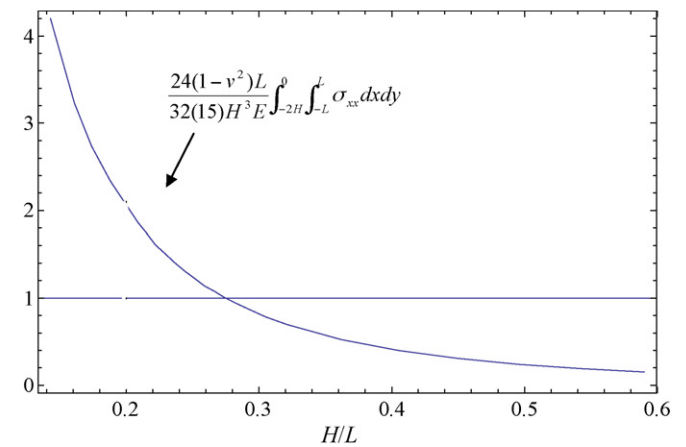
Rearrangement of terms results in the cancellation of elastic constants or

$$\frac{24(1 - \nu^2)L}{32(15)H^3E} \int_{-2H}^{0} \int_{-L}^{L} \sigma_{xx} dx dy = 1 \tag{9}$$

Eq. (9) predicts that the normalized average stress must be less than 1 in order for the particle to be attached on the substrate surface. Plotting therefore the left hand side of Eq. (9) as a function of H/L, it is found that it intersects the constant 1 at an aspect ratio of approximately 0.3, as indicated by Fig. 8. It should be noted that the elastic constants of Eq. (9) algebraically cancel and do not influence the solution.

The implication here is that for a given percentage of volume change during cycling, an island structure has a greater mechanical stability than a thin film, with $H/L = 0.3$ being the stability limit; aspect ratios above this limit increase the stability of island attachment on the substrate during cycling. This is consistent with the evidence of Fig. 4, which shows severe fracture of a Sn thin film during the first cycle. For the case where 8 wt% Sn is attached in the form of SnO₂ on Vulcan carbon, the representative SnO₂ island in the white circle in Fig. 5 has a height of 2.86 nm and a width of 5.2 nm, which indeed gives a H/L ratio of 0.55, which is the above theoretical limit that will inhibit fracture. Furthermore, the islands in black circles have a $H/L = 1$, which again inhibits fracture. Therefore, fracture was avoided for this material and a high capacity retention was obtained [9].

5. Conclusions

In the present study it was illustrated that continuum mechanics formulations can be adapted to examine fracture and damage evolution in next-generation anodes for rechargeable Li-batteries. This is important as the electrochemical performance of these power sources is directly related to their mechanical stability. In the first part it was shown that according to Fig. 3 lower Si volume fractions embedded in a less active matrix experience less cracking and therefore the anode maintains a higher mechanical integrity and a better capacity retention would be expected. This was shown to be in agreement with Si-SGG nanocomposite anodes [7], as indeed the anode with the lowest Si volume fraction showed better capacity retention than the anodes containing higher Si volume fractions.

In the second part of this paper experimental evidence on the mechanical failure of Sn thin film anodes motivated the study of the mechanical stability in nanoscale island structures. Application of linear elasticity indicates that the aspect ratio of the Sn islands plays an important role in maintaining the mechanical integrity of

the anode during cycling. The theoretical prediction reveals that retaining a H/L ratio greater than 0.3 will inhibit detachment of the Sn islands. This was found to be in agreement with the microstructure of a SnO_2/C anode, whose SnO_2 islands had a $H/L \sim 0.5–1$ and gave a stable capacity for over 300 cycles [9], whereas a continuous Sn layer fractured severely after the first cycle as shown in Fig. 4. It should be noted that other studies (e.g. [31]) have also indicated that Sn based thin films exhibit a poor capacity retention and attributed it to fracture. However, TEM and SEM images documenting this during the first cycle or a detailed theoretical analysis describing the underlying damage mechanics have not been presented before.

In concluding, it should be noted that in addition to volume size and aspect ratio of the particles, particle size also plays a significant role in fracture, as first noted by [32]. Such theoretical considerations are currently being undertaken.

Acknowledgment

References

[1] K.E. Aifantis, S.A. Hackney, R.V. Kumar (Eds.), High Energy Density Lithium Batteries: Materials, Engineering, and Applications, Wiley-VCH, 2010.
[2] R. Fong, R.U. von Sacken, J.R. Dahn, J. Electrochem. Soc. 137 (1990) 2009.
[3] J. Wang, I.D. Raistrick, R.A. Huggins, J. Electrochem. Soc. 133 (1986) 457.
[4] L.Y. Beaulieu, K.W. Eberman, R.L. Turner, L.J. Krause, J.R. Dahn, Electrochem. Solid-State Lett. 4 (2001) A137.
[5] Z. Wang, W. Tian, X. Li, J. Alloys Compd. 439 (2007) 350.
[6] J. Graetz, C.C. Ahn, R. Yazami, B. Fultz, Electrochem. Solid-State Lett. 6 (2003) A194.
[7] J. Niu, J.Y. Lee, Electrochem. Solid-State Lett. 5 (2002) A107.
[8] G. Derrien, J. Hassoun, S. Panero, B. Scrosati, Adv. Mater. 19 (2007) 2336.
[9] K.E. Aifantis, S. Brutti, S.A. Hackney, T. Sarakonsri, B. Scrosati, Electrochim. Acta 55 (2010) 5071.
[10] J.L. Gomez Camer, J. Morales, L. Sanchez, Electrochem. Solid-State Lett. 11 (2008) A101.
[11] A. Caballero, J. Morales, L. Sanchezz, Electrochem. Solid-State Lett. (2005).
[12] I. Kim, G.E. Blomgren, P.N. Kumta, Electochem. Solid-State Lett. 7 (2004) A44.
[13] Y.S. Jung, K.T. Lee, S.M. Oh, Electrochim. Acta 52 (2007) 7061.
[14] J. Wolfenstine, J. Power Sources 79 (1999) 111.
[15] R.A. Huggins, W.D. Nix, Ionics 6 (2001) 57.
[16] W.D. Nix, Metall. Trans. 20A (1989) 2217.
[17] K.E. Aifantis, S.A. Hackney, J Mech. Behav. Mater. 14 (2003) 403.
[18] K.E. Aifantis, J.P. Dempsey, J. Power Sources 143 (2005) 203.
[19] K.E. Aifantis, J.P. Dempsey, S.A. Hackney, Rev. Adv. Mater. Sci. 10 (2005) 403.
[20] K.E. Aifantis, J.P. Dempsey, S.A. Hackney, J. Power Sources 165 (2007) 874.
[21] Y. Shao-Horn, S.A. Hackney, A.J. Kahaian, K.D. Kepler, E. Skinner, J.T. Vaughey, M.M. Thackeray, J. Power Sources 81–82 (1999).
[22] (a) J. Christensen, J. Newman, J. Solid State Electrochem. 10 (2006) 293;
(b) J. Christensen, J. Newman, J. Electrochem. Soc. 153 (2006) 1019.
[23] M. Doyle, T.F. Fuller, J. Newman, J. Electrochem. Soc. 140 (1993) 1526.
[24] S. Golmon, K. Maute, M.L. Dunn, Comp. Struct. 87 (2009) 1567.
[25] J.P. Dempsey, L.I. Slepyan, I.I. Shekhtman, Int. J. Fract. 73 (1995) 223.
[26] J.P. Dempsey, A.C. Palmer, D.S. Sodhi, Eng. Fract. Mech. 68 (2001) 1961.
[27] K. Adpakpang, T. Sarakonsri, K.E. Aifantis, S.A. Hackney, (Submitted for publication).
[28] D.B. Marshall, A.G. Evans, J. Appl. Phys. 56 (1984) 2632.
[29] A.G. Evans, J.W. Hutchinson, Int. J. Solids Struct. 20 (1984) 455.
[30] R.W. Little, Theory of Elasticity, Prentice-Hall, 1973.
[31] N. Li, C.R. Martin, B. Scrosati, J. Power Sources 97 (2001) 240.
[32] J. Yang, M. Winter, J.O. Besenhard, Solid State Ionics 90 (1996) 281.